

OPTICAL MEASUREMENTS FOR THE FLYBY NAVIGATION OF ROSETTA AT ASTEROID STEINS

Mathias Lauer⁽¹⁾, Ulrich Herfort⁽²⁾, Dave Hocken⁽³⁾, Sabine Kielbassa⁽⁴⁾

*(1) ESA/ESOC/OPS-GFI, Robert-Bosch-Strasse 5, 64293 Darmstadt, Germany,
+49(0)6151-902902, Mathias.Lauer@esa.int*

*(2) EDS, ESA/ESOC/OPS-GFI, Robert-Bosch-Strasse 5, 64293 Darmstadt, Germany,
+49(0)6151-902132, Ulrich.Herfort@esa.int*

*(3) VCS-SciSys, ESA/ESOC/OPS-GFI, Robert-Bosch-Strasse 5, 64293 Darmstadt, Germany,
+49(0)6151-902463, Dave.Hocken@esa.int*

*(4) EDS, ESA/ESOC/OPS-GFI, Robert-Bosch-Strasse 5, 64293 Darmstadt, Germany,
+49(0)6151-902701, Sabine.Kielbassa@esa.int*

ABSTRACT

The ESA interplanetary S/C Rosetta was launched in March 2004 to rendezvous with comet Churyumov-Gerasimenko in 2014. The overall trajectory contains four planetary swingbys, three at Earth and one at Mars. The scientific outcome of the mission is enhanced by two asteroid flybys, one occurred in September 2008 at asteroid Steins, and the second is foreseen in 2010 at asteroid Lutetia, after the last Earth swing-by.

For the Steins flyby, optical measurements taken by on-board CCD cameras were used to navigate the S/C towards the requested flyby conditions and to autonomously control the attitude of the S/C during the flyby phase proper in order to ensure that scientific instruments were accurately pointing to the asteroid. The two different phases, i.e. the approach phase and the flyby phase, created different challenges to the operational on-ground support which are addressed in this paper, together with post-flyby analyses of the eventually achieved results.

1. CHARACTERISTICS OF S/C, ASTEROID AND ORBITS

An overview of the S/C geometry is given in fig. 1. The S/C consists of a box shaped body which measures 2.1 m, 2.0 m and 2.6 m along the three axes. Two solar arrays (SA) of 2.3 m width and 14.4m length are attached to the +y and -y faces of the S/C body. They can be rotated around the S/C y axis. A moveable high gain antenna (HGA) dish with 2.2 m diameter is mounted on the S/C body. It can be rotated in two axes around a pivot point on a tripod assembly at the lower corner of the S/C. This provides the HGA with greater than hemispherical coverage.

The attitude of the S/C is estimated on board using autonomous star trackers with 16° field of view size and three inertial measurement units with three perpendicular ring laser gyros each. The attitude is controlled using four reaction wheels with 39 Nms angular momentum capacity. A bipropellant reaction control system with a redundant set of eight balanced 10 N thrusters serves for wheel off loadings and attitude control in safe mode. An additional redundant set of four 10 N thrusters mounted on the -z face of the body, with thrust direction close to +z, is used for orbit control manoeuvres.

Nominal Earth communication is accomplished through the HGA in X band. Additional medium and low gain antennas can be used for special operations or in contingency cases.

The dry mass of the total S/C is 1343 kg. At launch, the tanks were filled with 1059 kg oxidizer, 660 kg fuel and 5 kg pressurant gas.

For optical navigation, two navigation cameras (NAVCAM) are mounted on the S/C body with boresights pointing towards the +z direction. This is also the direction along which important payload instruments are pointing. This payload comprises the OSIRIS narrow angle (NAC) and wide angle (WAC) optical cameras, a UV spectrometer (ALICE), a microwave sensor (MIRO) and an imaging spectrometer (VIRTIS).

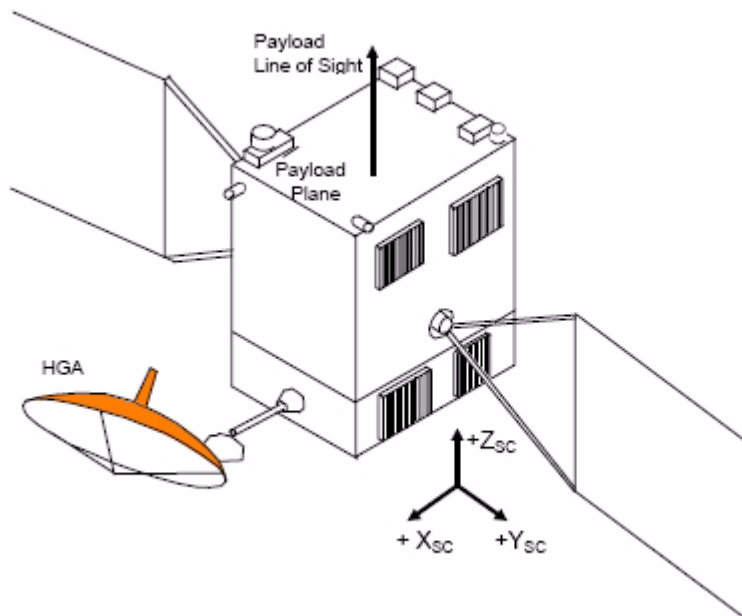


Fig. 1. Rosetta Spacecraft Geometry

The main characteristics of the optical cameras are shown in table 1 (for the science cameras, the characteristics have been compiled with the support of the OSIRIS experiment team, e.g. using data from [6] and [7]). The NAVCAMs are the nominal instruments for the S/C operation (orbit navigation and attitude control). However with the Steins flyby, additional processing of images from the OSIRIS science cameras for S/C operations was exercised for the first time in the Rosetta mission. It is foreseen to re-use this interface as well for the Lutetia flyby in 2010 and the comet phase starting in 2014. The main advantages of the science cameras relevant for operations are the high angular resolution of the NAC (for optical navigation), the large field of view of the WAC (for comet mapping), the high dynamic range and resolution of the CCD and the low noise due to its 160 K CCD operating temperature.

The overall geometry of the flyby was already given by the interplanetary trajectories of the S/C and the asteroid (a detailed description of the S/C and asteroid orbits is given in [1]). As a result of the trajectory optimization, the nominal time of closest approach (CA) was at 18:38:16 UTC on September 5, 2008. The Sun distance at this time was 2.1 AU and the Earth distance 2.4 AU which is equivalent to a one-way light time of 20 minutes. The flyby speed was 8.616 km/s. The diameter of Steins was predicted to be in the order of 4.5 km (see e.g. [4]), with an axial ratio of 1.3. Magnitude parameters were available from several sources based on recent measurements at various phase angles from Earth based telescopes and also from images taken by a science camera on-board the S/C (see e.g. [2] and [3]). As best pre-flyby estimates an absolute magnitude of $H=13.3$ and a slope parameter of $G=0.3$ were used (these parameters refer to the standard magnitude system for asteroids, which is given e.g. in [5]).

Table 1: Camera Characteristics

Parameter	NAVCAM	OSIRIS/NAC	OSIRIS/WAC
Optics type	7 lenses, 3 filters	3 mirrors off-axis, dual filter wheel	2 mirror off-axis, dual filter wheel
Aperture diameter	7 cm	9 cm	2.5 cm
Field of view	5° x 5°	2.20° x 2.22°	11.34° x 12.11°
Focal length	152.5 mm	717.4 mm	136 mm
CCD	1024 x 1024 pixels	2048 x 2048 pixels	2048 x 2048 pixels
Equiv. pixel size	5 mdeg	1 mdeg	6 mdeg
Full well	70,000 el	100,000 el	100,000 el
Signal resolution	12 bit: 0-4095	16 bit: 0-65535	16 bit: 0-65535
CCD Temperature	-10 +/- 10 degC	160K to 300K	160K to 300K

In terms of flyby conditions, the only remaining adjustable navigation parameters were the flyby distance (i.e. the distance at the time of CA) and the orientation of the flyby plane (i.e. the plane defined by the asteroid and the relative motion of the S/C). The scientific community asked for the smallest possible flyby distance and for a minimum phase angle (Sun-asteroid-S/C angle) of 0° to occur during the flyby. The latter request determined the orientation of the flyby plane in order to contain the Sun line. As the payload instruments are mounted fixed on the central body of the S/C, the S/C had to perform a fast rotation over the flyby to keep the payload boresights pointing towards the target. The dynamical constraints of the AOCS in terms of maximum angular rates, maximum torques on the reaction wheels etc. allowed, together with the given flyby speed, to select a minimum flyby distance of 800 km.

2. APPROACH PHASE

The approach phase started beginning of August 2008, slightly more than one month prior to CA. The a-priori knowledge of the asteroid position at CA derived from orbit determination based on telescope observations was in the order of 100 km (1σ) in each component which was not sufficient for navigation. In order to improve the relative position estimate in the target plane at CA (the plane perpendicular to the relative flyby velocity) the additional usage of optical measurements was required.

The Sun-S/C-asteroid angle was 160° in July 2008 and dropped down to 142° at 12 hours before CA. This was well within the operational range for the NAVCAM, which requires a Sun angle from the boresight of more than 60°. The phase angle, or Sun-asteroid-S/C angle, was 16.5° in July 2008 and increased up to 38.2° at 10 hours before CA. This range of phase angles was covered by the Steins magnitude measurements that were used to derive the nominal magnitude parameters (see above). It was therefore expected that the magnitude predictions based on the nominal model were accurate enough for operational purposes, which was confirmed by the actual images taken during approach.

The predicted brightness during approach is shown in fig. 2. The nominal detection limit of the NAVCAM is 11mag. This limit was reached ca. 20 days prior to CA. However, it turned out that the

asteroid could already be reliably detected for the first time on 4 August, i.e. 32 days prior to CA in an image taken with 30s exposure time at a distance of 24 Mio km with an asteroid magnitude of close to 12 mag. One day prior to CA, when the last images for navigation purposes were taken, the magnitude of Steins was 3.2 mag. Over the period of the navigation campaign, the signal of the asteroid in the images therefore varied by a factor of ca 3,300.

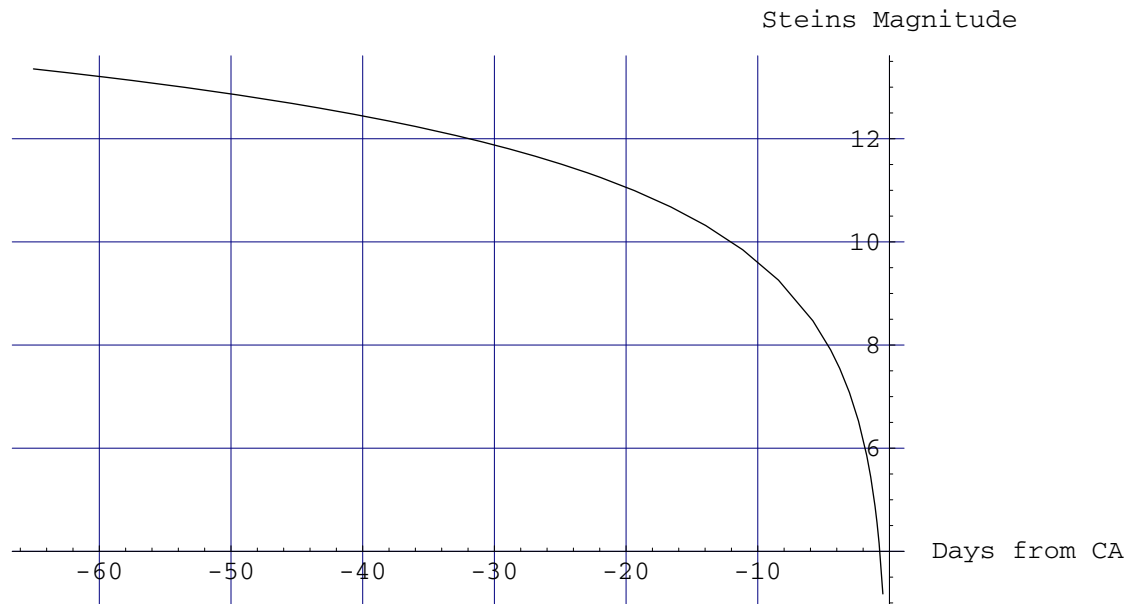


Fig. 2. Asteroid Brightness during Approach

The apparent motion of the asteroid as seen from Rosetta before CA in the plane of sky is shown in fig. 3. The position is indicated by a circle every day from 65 days until 1 day before CA. The size of the circle indicates the apparent brightness as seen from the S/C. In addition, all stars from the Hipparcos and Tycho catalogue are drawn as circles. Their magnitudes are specified below the circle and are also used to scale the circle size.

The asteroid apparent magnitude at CA - 65 days was fainter than the limiting magnitude of the catalogues. Therefore, considerably more stars with magnitude similar to that of the asteroid would be visible in this field of view.

There was a turning point in the apparent motion slightly more than 4 days before CA. At CA - 65 days, the asteroid is moving with ca. 40 mdeg/day, or equivalently 8 NAVCAM pixels/day, with decreasing right ascension and increasing declination. This rate gradually decreased to almost zero at the turning point. After the turning point, the apparent position was again accelerating reaching a speed of 2.5 mdeg/hour, or equivalently 0.5 pixels/hour, at 1 day before CA.

The apparent position of Steins was always sufficiently far away from the stars, such that overlapping of the target signal with a star signal in an image could not occur. The closest angular distance was 84 mdeg, or equivalently 17 NAVCAM pixels. This minimum distance was reached with Tycho star (4979,800,1) at the turning point, i.e. slightly more than 4 days before CA. At this time, the apparent brightness of the asteroid was already 7.8, i.e. more than 4 magnitudes brighter than the star.

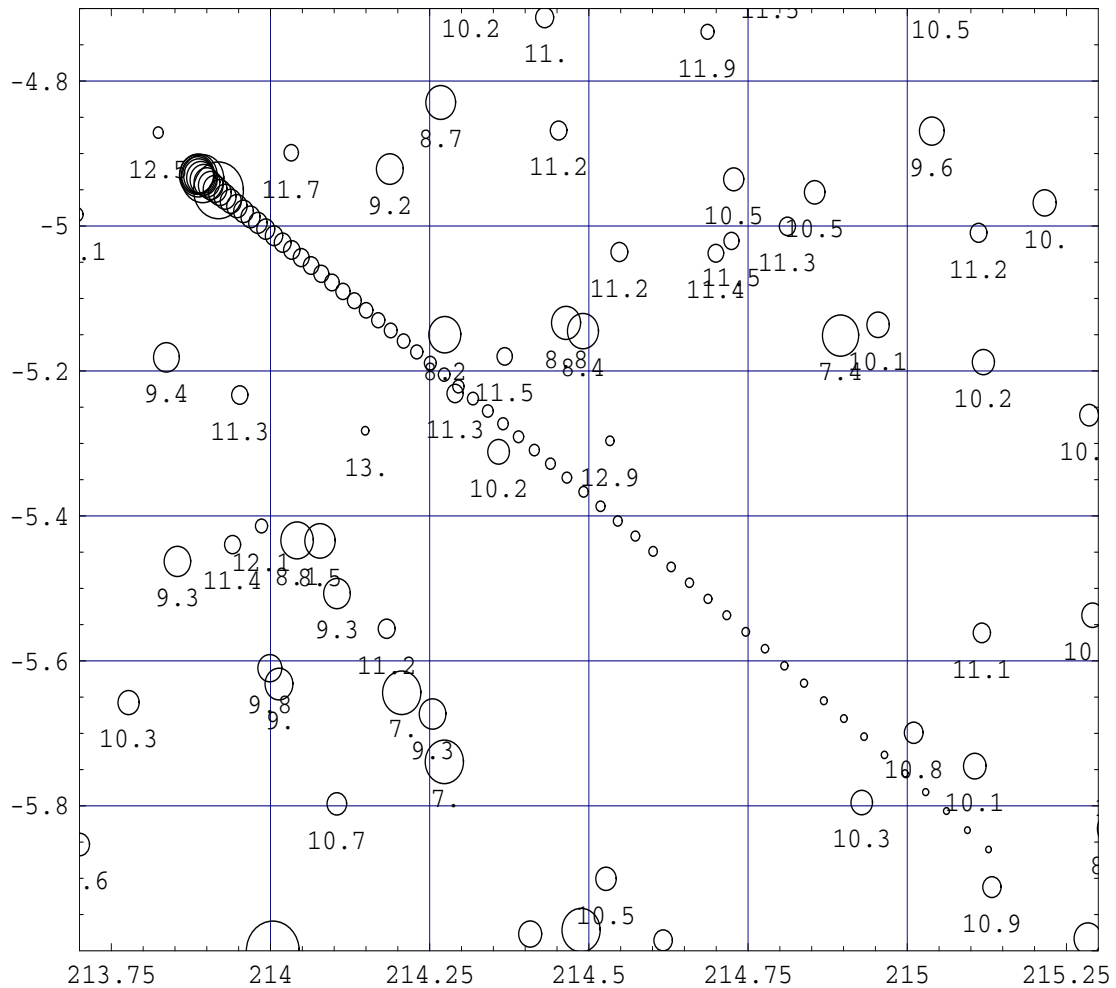


Fig. 3: Steins apparent motion from CA - 65 days to CA - 1 day
horizontal axis: right ascension (deg) / vertical axis: declination (deg)

The nominal dynamic range of the NAVCAM is 3.56 magnitudes. Within the field of view radius around the Steins direction at 11 days before CA, 104 stars from the Hipparcos and Tycho catalogue brighter than visual magnitude 10 are visible. The distribution of magnitudes is not equal over the full range required for the navigation, i.e. between the faint limit of 11 mag and the bright limit of 3.2 mag. Almost all stars have magnitudes in the range from 7 to 10. For the last images containing a bright target only 5 stars with magnitudes brighter than 6.76 (= Steins faint limit of 3.2 plus dynamic range of 3.56) could be used for image processing.

For relative navigation, the simultaneous determination of S/C and asteroid orbits was based on optical measurements, in addition to standard radiometric data (this process is described in detail in [1]). One optical measurement is derived from an image and consists of the direction given as right ascension and declination from the S/C to the asteroid. The images were taken during dedicated observation slots. In the weeks CA-5 to CA-3, two observation slots per week were allocated. During the last two weeks until CA-1 day, daily observation slots were performed. During one observation slot, with a typical duration of 4 hours, 10 NAVCAM images from each unit and 5 OSIRIS/NAC images were acquired. The number of images was a trade-off between accuracy and robustness versus data volume. With a higher number of images, the number of measurements increases and therefore the statistics are improved. Images disturbed by spurious events could be discarded without losing an observation slot. A range of integration times could be used, rather than a single exposure duration,

such that the best images, e.g. in terms of residual error in the star directions, could be selected. The number of images was however limited by the maximum achievable data rate and the required processing time on ground between data acquisition and subsequent execution of an orbit correction manoeuvre (OCM). The allocated slots for these manoeuvres are shown in table 2.

Table 2: Orbit Correction Manoeuvre Slots

Date	Days from CA	Optical Data Cut-off prior to OCM	Delta-v
2008/08/14	- 3 weeks	- 3 days	12.8 cm/s
2008/08/28	- 8 days	- 3 days	not used
2008/09/02 15:30	- 3 days	- 32 hours	not used
2008/09/04 04:00	- 36 hours	- 20 hours	11.8 cm/s
2008/09/05 06:00	- 12 hours	- 13 hours	not used

The table shows that, for the last slot at CA-12 hours, the total manoeuvre preparation time, including transmission of image data to ground, data reduction, orbit determination, command generation and upload of commands with back-up opportunity, was only 13 hours.

For the reduction of the images, the processing cycle comprised the following main steps. In a first step, the mean background was determined and all pixels with significant electron content, e.g. 3σ noise level above the mean background. Then all pixels with significant signal belonging to the same object were identified. The list of resulting objects was filtered for several criteria. Objects with a too low number of pixels, or with saturated pixels were rejected. In the next step, the centre position of all objects was determined. There were several methods available, one dimensional and two dimensional fits, parabolic and Gaussian object shape models, averaging methods (photometric, geometric), various window sizes (e.g. 3 by 3 or 5 by 5 pixels around the maximum, or full window over all significant pixels). The best results were achieved with one dimensional Gaussian fits over 3 pixels for the NAVCAM, and with the photometric averaging method using a 5 by 5 pixel window for the NAC, although the dependency on the centroiding method was not very strong for both cameras. After the centroiding, the object centre positions were converted from pixel values to directions in camera frame. In this step, a distortion correction was applied. For the NAVCAM, the distortion model consists of a polynomial with contributions up to order 5. Using the a-priori knowledge of the camera attitude (based on star tracker measurements and relative alignment data), a few bright objects on the CCD were matched against the Hipparcos star catalogue and the initial attitude estimate refined. This intermediate step was necessary as the initial attitude knowledge based on star tracker data was not sufficiently accurate for the final star matching. Based on the refined attitude, for all objects a matching was tried against the combined Hipparcos and Tycho star catalogues. A matching was considered successful only if there was a unique star within a search area around the object and if this unique star was closer than a given matching distance. With this rule, a mismatching in regions containing several stars within a small area was avoided. The size of the search area and the matching distance were configurable. For the comparison of the star and object directions, proper motion and stellar aberration were applied to the star positions in the catalogue. The result of this step was a list of pairs of directions, one in camera frame for the image object and one apparent in inertial frame for the matched star. In the final step, a camera attitude was determined which minimized the residuals of the angular separations for each pair. In this step, the algorithm could also reject a star based on the resulting residual. By this, measurements disturbed by noise or a spurious event could be filtered out. Based on the final attitude, the apparent direction of the asteroid was

determined from its direction in camera frame. For the final input to the orbit determination, the apparent inertial direction was corrected for stellar aberration (a correction for light time was not applied, since this is considered in the orbit determination software).

In preparation of the Steins flyby navigation and as validation of the image reduction process, test images of the star background were already acquired by the NAVCAMs in December 2007 with various integration times. Instead of Steins, six stars in the field of view with magnitudes between 4 and 11 were treated as target with known inertial direction from the star catalogue. The images were used to tune the processing parameters (e.g. threshold for pixel detection, centroiding method, search area for matching and maximum match distance, optimization parameters), and to find an estimate for the achievable measurement accuracy. It was found that, with the optimum setting, the residuals were all well below one tenth of a pixel, i.e. below 0.5 mdeg.

For the semi-major and semi-minor axes of the 1 sigma error ellipsoid in the relative position of the asteroid perpendicular to the line of sight from the S/C to the target, values of ca. 100 km and 60 km were estimated prior to the approach phase. A 0.1 pixel accuracy for the optical measurements with the NAVCAM would correspond to 100 km at ca. 11 days before CA. With the NAVCAM, only at this date, the optical data would improve the relative orbit estimate. However, in addition to the NAVCAM, images of the science camera (OSIRIS/NAC) could be used. From the characteristics listed in table 1, the angular resolution of the NAC is ca. 5 times higher than that of the NAVCAM, such that 5 times better accuracies in the NAC optical measurements was expected. This was confirmed in flight with the first operational images, such that the optical data could improve the orbit determination already from the beginning of the observation campaign.

The residuals of the optical measurements derived from the NAVCAM images are shown in fig. 4. The residuals are based on the post-flyby final result of the orbit determination using radiometric and optical data (see [1]). The residuals are as expected almost all below one tenth of a pixel (0.5 mdeg). Similarly, the NAC residuals are nearly always below one tenth of a pixel (0.1 mdeg). The mean values and standard deviations of all residuals are given in table 3.

Table 3: Residuals of Optical Measurements

Camera	Right Ascension (mdeg)	Declination (mdeg)
NAVCAM 1	-0.107 +/- 0.177	0.014 +/- 0.231
NAVCAM 2	-0.040 +/- 0.178	-0.064 +/- 0.230
OSIRIS/NAC	0.002 +/- 0.054	0.024 +/- 0.047

The individual residuals in fig. 4, however, show that their distribution around the mean is not fully random. Instead, often all measurements in one component of the same camera unit are biased towards the same side of the mean. For example, in the measurements of the observation slot at CA -22 days, the right-ascension and declination residuals for camera unit 1 are all positive, whereas all residuals for camera unit 2, with one exception, are all negative. Such a bias can be seen in fig. 4 at almost all observation slots. This bias for one component and one camera is not the same in all observation slots. For example the bias in the declination residuals for camera unit 2 is positive for the slots at -32 and -18 days from CA, and negative for the slots at -29, -26, -22, -16 days from CA. Similar biases were seen in the results from the OSIRIS/NAC camera. This effect is probably due to the nature of the measurement. The direction measurement of an object detected on the CCD of a camera has several error components. There are errors which are due to temporal noise (e.g. from

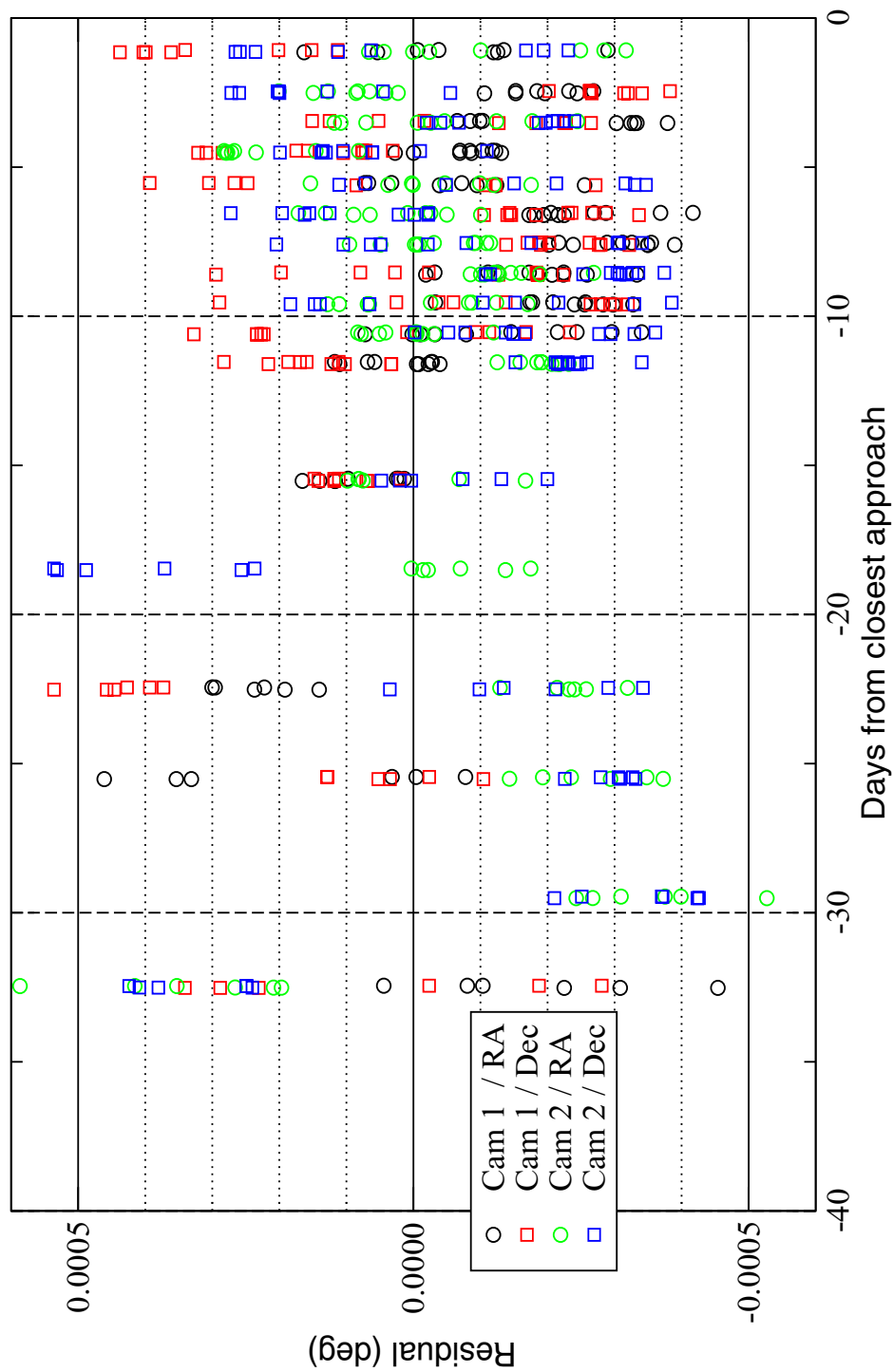


Fig. 4: Residuals of optical measurements from NAVCAM images

statistical fluctuations in the electron content of a pixel), and errors which are systematic for a fixed position on the CCD, but random when all positions on the CCD are considered. To this type of error

belongs the residual error of the distortion correction. Therefore, if the object is repeatedly measured at the same position on the CCD (as during the images in one observation slot), the resulting direction will show a systematic bias on top of the statistical noise error. If the object is measured at various positions on the CCD (as for the case of considering all optical measurements of a camera unit over the full navigation campaign), these biases appear as random. As images from three camera units were used in each observation slot, the individual biases were cancelling to some extent, although the bias in the NAC data was dominating due to the higher accuracy.

3. FLYBY PHASE

The flyby geometry is shown in fig. 5. The asteroid is depicted as a red sphere and the S/C is flying by on a straight line from left to right. The plane of the figure is the flyby plane, i.e. the plane defined by the asteroid and the orbit of the S/C relative to the asteroid. The direction towards the Sun is also contained in this plane and shown as a red arrow. The S/C is passing by on the Sun side and is observing the target with 0 phase angle ca. 2 minutes prior to CA. In order to maintain the payload boresight (= S/C z-axis shown as black arrow) pointing towards the asteroid over the flyby phase, the S/C had to rotate around its y-axis.

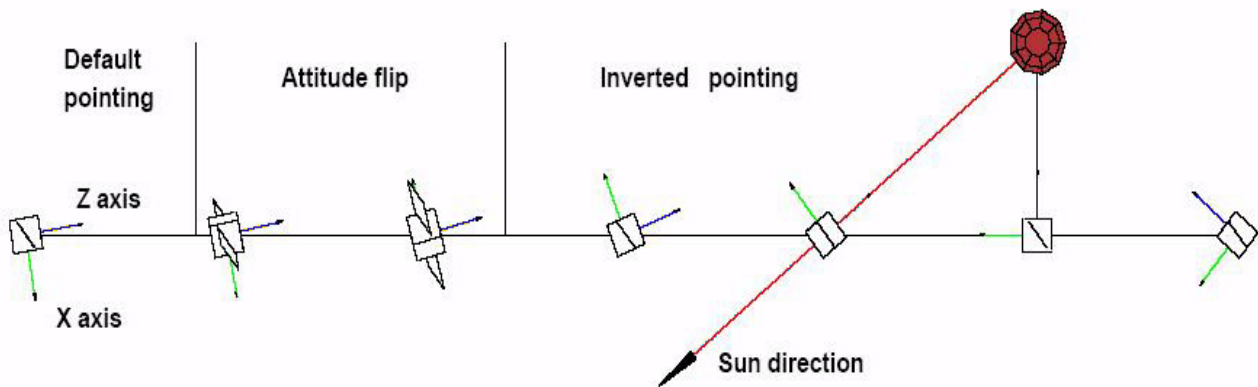


Fig. 5: Flyby Phase

With the help of optical measurements during approach, the S/C was navigated accurately to the impact point in the target plane (i.e. plane through the asteroid, perpendicular to the relative flyby velocity). The nominal target was defined by a flyby distance of 800 km and the requirement that the phase angle should pass through 0° during flyby. The finally achieved flyby distance was 802.6 km and the minimum phase angle 0.27° . The relative position along the flyby trajectory was however not known on ground prior to CA very accurately (the initial estimate of the time of CA was 18:38:05 UTC with an uncertainty of 18.5 seconds). This knowledge could hardly be improved during approach, as the optical measurements essentially determined the position of the asteroid only in the target plane. A S/C attitude following a guidance uploaded from the ground would therefore not be sufficient for precise payload pointing. The AOCS therefore switched twenty minutes prior to CA into a dedicated asteroid flyby mode (AFM), where autonomously the position of the asteroid was determined by the NAVCAM, and the S/C attitude adjusted accordingly. At AFM entry, the error in the tracking angle (angle between flyby direction and pointing direction) was still very small (ca. 3 mdeg, i.e. below one NAVCAM pixel), the error in the out-of-plane angle had already reached 33 mdeg.

Already twelve hours prior to CA, the NAVCAM was commanded for the first time, outside the AOCS control loop, into asteroid tracking mode for check-out purposes. This camera mode was designed especially for tracking an extended target, and was successfully tested during the first Earth swing-by in March 2005 with the Moon as target. In this mode, the camera autonomously selects the exposure parameters (integration time, gain, detection threshold etc.) and periodically determines the direction of the target from the images that are acquired every 2.5 s. At this time, the expected magnitude of Steins was 3.3 and its apparent size still less than 1 pixel. A window of 100 x 100 pixels was commanded to the camera to detect the asteroid and measure its direction. But instead of only a few pixels (due to the optics, the signal from the asteroid would extend over a matrix of several pixels), the camera reported in telemetry (TM) a nearly constant number of ca. 60 pixels within the 100 pixel window, which corresponds to a ratio of detected pixels per total number of window pixels of 0.60%. I.e. almost all of the detected pixels could not belong to Steins. And instead of 3.3, the magnitude of the object was reported in TM to be around 4.8.

The detection threshold was autonomously set by the camera to ca. 36 digital units (DU's), where 1 DU corresponds to 17 electrons. The brightest stars in the field of view were of magnitude 7. Such a star generates a signal of ca. 9 DU's. The detected pixels could therefore also not belong to stars. For further analysis, 5 images (see one example in fig. 6) were acquired and processed on ground.

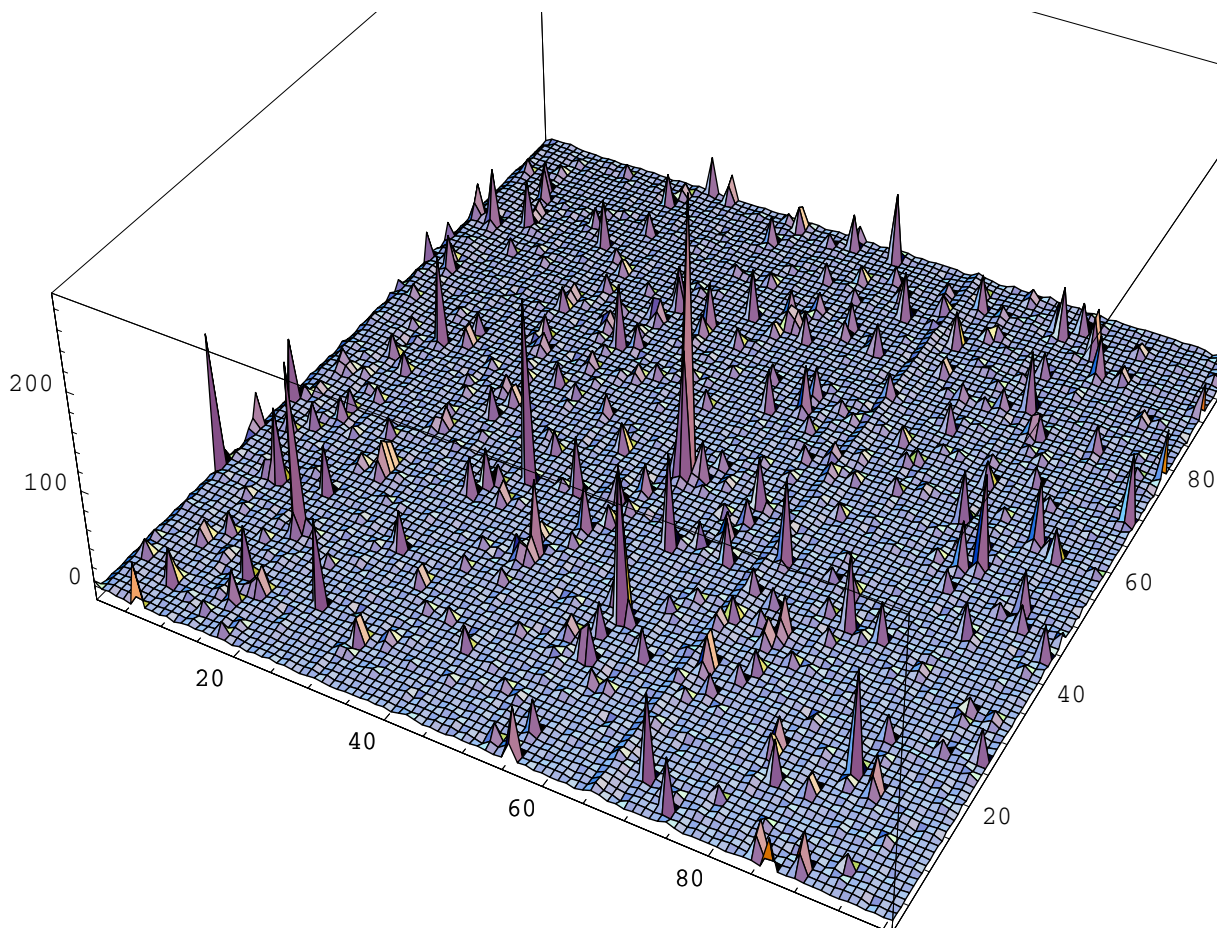


Fig. 6: NAVCAM Image in Tracking Mode

In the images, Steins could be clearly identified in the centre of the window. It extended over four pixels with a signal above the detection limit. The position of these pixels was within 1 pixel of the expected position of Steins. The average total signal of Steins from all 5 images was 505 DU's, which was also consistent with the expected total signal.

The images however also showed clearly a number of ca. 50 warm pixels with a signal exceeding the detection limit (i.e. 36 DU's above the mean background) that disturbed the target identification. This was consistent with the number of detected pixels as reported in TM. Their average signal rate in the 100 x100 pixel window was 30 DU/s, which explained the fainter magnitude (4.8 instead of 3.3) of the tracked object reported in camera TM.

It was clear that the determination of the object centre position of the asteroid by the camera was affected by the warm pixels. This position is determined by the camera as the average position of all detected pixels, with all positions weighted with the corresponding pixel signal. A rough estimate of this disturbance can be derived under the assumption that the warm pixels are evenly distributed over the CCD with an average density of 60 per 100x100 pixels and an average signal rate of 30 DUs/s. In this case, and in the absence of a target, the object centre position would be determined exactly in the middle of the tracking window. With the asteroid in the window, the centre position of the object would be determined along each axis as a fraction of the asteroid position along this axis. This fraction is the ratio of the asteroid signal (i.e. the total signal of all pixels that belong to the asteroid) over the total signal (i.e. the total signal of all detected pixels, either asteroid or warm pixel). According to this simplified estimate, the disturbance would be very small in the beginning of the tracking period, as the nominal asteroid position was already at the centre of the tracking window. However, at 12:45 the S/C slewed to point with the MIRO boresight towards the asteroid, instead of the ALICE boresight, that had been pointed towards the asteroid until then. The window position of the camera was however not adjusted at this time. As a result of the slew, the asteroid position moved, w.r.t. the window centre, to $(-0.14^\circ, 0.09^\circ)$. The simplified estimate predicted a shift in the measured object centre away from the window centre by 24%, i.e. to $(-0.03^\circ, 0.02^\circ)$, which was exactly the mean shift seen at this time in TM. At 13:31, the tracking window was increased to 200x200 pixels, which is the value that was intended to be used at the start of the AFM. Based on the previous assumptions, the simplified analysis predicted a shift of the measured centre positions back towards the window centre, due to the increase of the number of warm pixels in the window by a factor of 4. This was indeed reported in TM.

The conclusion of the analysis was that the asteroid tracking over the test period was not successful, but considerably disturbed by the detection of warm pixels. It was also clear that this performance should improve during approach with the increase of the asteroid size and brightness. According to the mission management there was a flight rule, that a condition for enabling the autonomous S/C pointing mode was that the camera successfully tracks the asteroid at 16:00, i.e. ca. 2.5 hours before CA. In case of tracking failure, a ground commanded backup pointing would be enabled that was based on the latest flyby time estimate. It was however predicted that at this time the performance of the camera in terms of tracking accuracy would not reach its nominal performance. It was therefore considered too risky to stay with the nominal set-up of the camera and to enable AFM without successful tracking of the asteroid 2.5 hours prior to CA.

In the following a series of tests was carried out with the redundant camera unit, to find a setting that would allow successful asteroid tracking. The major modifications were the removal of the attenuation filter and the disabling of the automatic exposure control. The new filter increased the ratio of the signal from the asteroid compared to the signal of the warm pixels by a factor of ca. 557. The integration time was commanded to the smallest possible fixed value of 0.01 s. With this setting, the warm pixels were not detected anymore and the asteroid accurately tracked. At 16:00 the decision in favour of the autonomous pointing option was taken and the AFM mode enabled.

The drawback of the modified setting was, however, that the asteroid would overexpose for some time over the flyby. It was predicted, that for the maximum brightness, the illuminated pixels would exceed the saturation limit by a factor of ca. 14. According to a pre-flight test with the CCD, an

object that is overexposed by a factor of 100 appears extended on the CCD only by a factor of 1.55, such that the centre position measurement of the asteroid should not be affected considerably.

The actual performance of the tracking was analysed post flyby based on the final S/C and asteroid orbit reconstruction. The overall history of the error is shown in figs. 7 and 8.

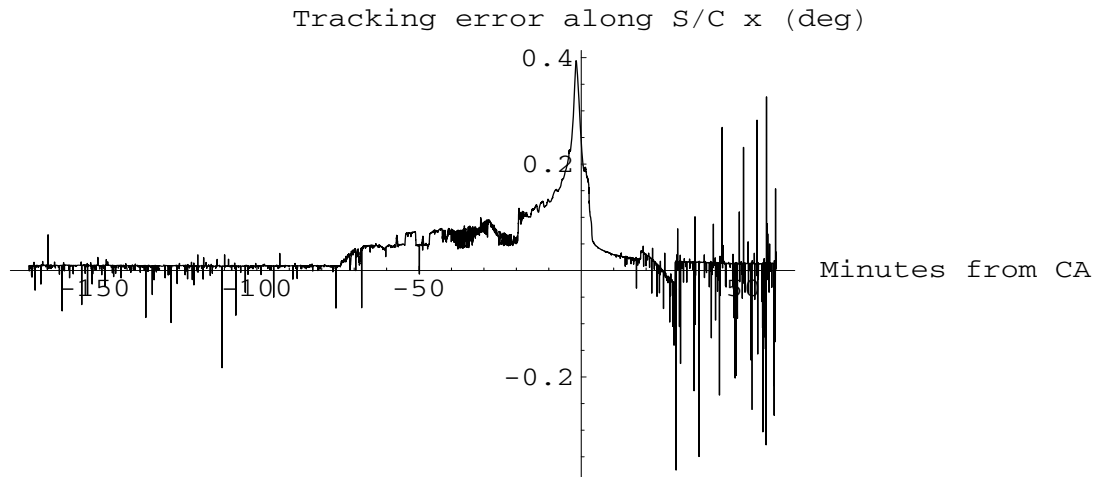


Fig. 7: NAVCAM Tracking Performance along S/C x-axis

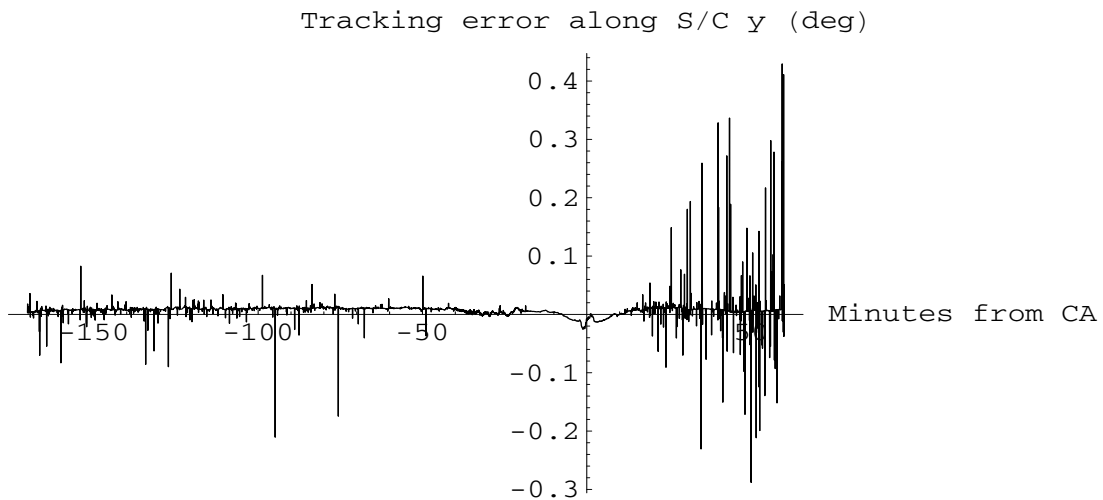


Fig. 8: NAVCAM Tracking Performance along S/C y-axis

The figures show the raw TM data which contain considerable noise. This noise is due to pixels with high electron contents caused by charged particles hitting randomly the 350 by 350 pixel window used for tracking. These pixels are considered part of the target by the autonomous camera processing software. The target centre position was therefore shifted randomly by an amount that depends on the position and signal of the disturbing pixel within the tracking window, and on the size and the apparent brightness of the asteroid as the target centre is determined by taking the average position over all target pixels where each pixel is weighted with its signal. The noise was considerably smaller around CA (from ca. CA -50 minutes onward until CA +10 minutes) where size and brightness of the asteroid reached its maximum. The biggest disturbance appeared after CA, where the asteroid size was decreasing and the phase angle approaching quickly a limit of ca. 140° . For the

S/C attitude control, the noise was filtered out by the on-board AOCS software, such that only the mean value was relevant for the pointing performance.

The tracking performance (after removal of the noise) is different for the two S/C axes. For the S/C y-axis (equivalent to the angle out of the flyby plane), the mean tracking error is always in the order of only 0.01° , or 2 pixels. For the S/C x-axis (equivalent to the tracking error in the flyby plane) the performance shows three clearly distinct periods:

Period 1: From the start of the tracking until ca. 17:25, i.e. ca. 75 minutes before CA, the asteroid is also tracked very accurately with a mean error of ca. 0.01° (i.e. 2 pixels).

Period 2: From 17:25 until 18:28 (i.e. 10 minutes before CA), the error gradually increases to ca. 0.1° . Subsequently, the error shows a sharp peak of 0.4° maximum until it drops again to ca. 0.05° about 3 minutes after CA.

Period 3: From 3 minutes after CA until end of AFM, the mean error drops again to ca. 0.02° .

The reason for the degraded performance in period 2 could not be identified without uncertainty, as it was not possible to store and download images taken by the tracking camera over the flyby. But there are indications that it is related to blooming of the CCD, i.e. the spill over of electrons from saturated pixels into columns. Fig. 9 shows the total number of detected pixels in the tracking window as reported in TM:

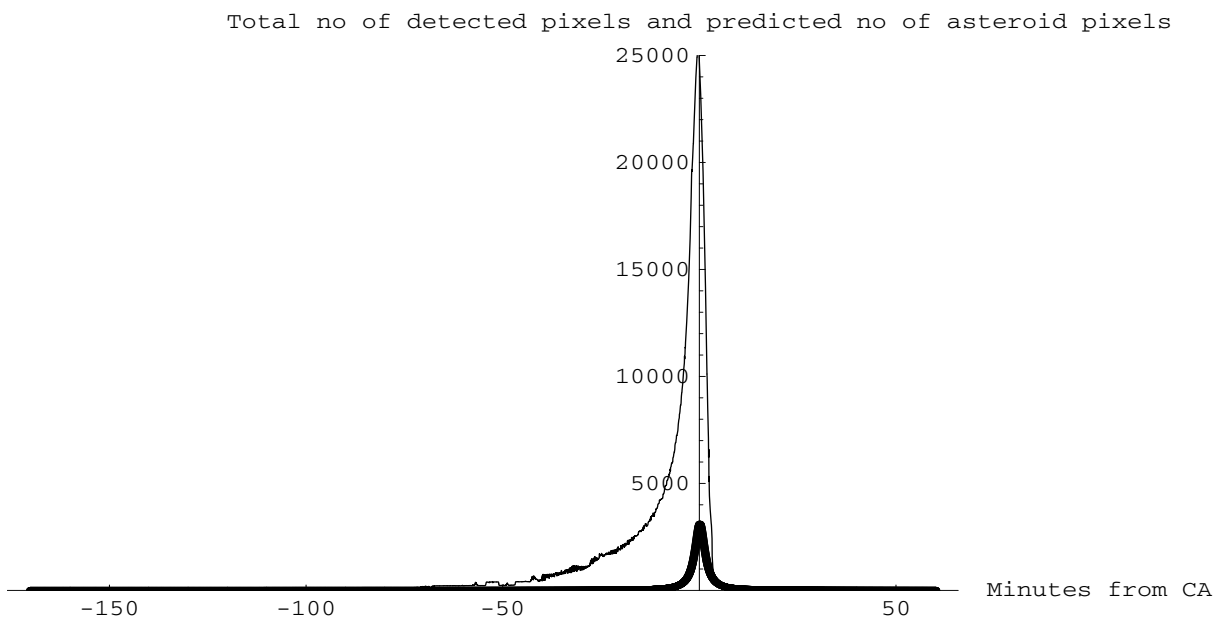


Fig. 9: NAVCAM Number of Detected Target Pixels

For comparison, the thick line in fig. 9 shows the number of detected pixels of the asteroid on the CCD as predicted based upon a fully illuminated sphere with 5 km diameter. From CA - 75 minutes onwards, the number of detected pixels starts to considerably exceed the number of predicted pixels from the asteroid. A magnification of the plot at the start of the increase shows, that the number of detected pixels increases in steps of approximately 170 pixels, which is about half the size of a column in the tracking window.

In addition, the envelope of the target (i.e. the smallest rectangular sub-window on the CCD that contains the target pixels) as reported in TM, extends until the start of period 2 in the mean only to a few pixels around the asteroid. Then at the start of period 2, the envelope suddenly extends along the -x axis of the CCD fully until the end of the tracking window. This indicates that from this time onward, all pixels in a column to the -x side of the asteroid on the CCD exceed the threshold for object detection. This effect lasts until the end of period 2. About 30 minutes later, at ca. 17:55, the envelope suddenly extends also to the +x limit of the tracking window, which indicates that then all pixels of the column exceed the detection threshold.

This behaviour was not expected. Although, in the operational case, the asteroid overexposure is considerably smaller than the one for the pre-flight CCD test, the number of detected pixels is considerably more increased than in the test. In addition, not only the object is extended, but also complete columns are apparently illuminated.

When the pixels, that are considered to be part of the tracked object, extend from the asteroid to the -x side of the tracking window, the average centre position is shifted towards -x on the CCD, or equivalently (due to inversion of the optics) the direction of the measured object centre along the +x axis of the S/C (the axes of the CCD and the S/C almost coincide). As the envelope shifts towards the +x side of the window considerably later than to the -x side, it is reasonable to assume that the signal in the pixels on -x side are higher than on the +x side, even when all pixels of the full column exceed the detection threshold. This again means that the average centre position is shifted towards -x on the CCD, or the direction along the +x axis of the S/C.

The overall pointing accuracy of the payload boresight over the flyby did therefore not fully reach the expected performance. The pointing error out of the flyby plane remained always below 0.01° , whereas the maximum in-plane error (i.e. error in the tracking angle) was 0.4° , compared to an overall requirement of 0.3° .

4. CONCLUSION

For the first time, an ESA S/C was navigated using optical data from on-board cameras, in addition to radiometric data.

During approach, the optical line of sight measurements from the S/C to the asteroid, based on images of the asteroid against the star background, reached an accuracy of ca. 0.1 pixel, which translates into 0.5 mdeg for the NAVCAM and to 0.1 mdeg for the OSIRIS/NAC. Based on these measurements the achieved flyby distance in the target plane was off from its nominal value by only 2.6 km, and the minimum phase angle only by 0.27° . The measurements did not appear completely random, but showed a bias dependent on the camera unit and the observation slot. It is suspected that this error is due to the random bias of the cameras. This is a measurement error type that depends on the position of the target on the CCD and that cannot be removed by averaging over several images.

The performance of the navigation camera in autonomous asteroid tracking mode was not fully nominal. With the nominal setting, the camera could not successfully track Steins during the verification period prior to the entry into the autonomous S/C pointing mode on the 5th of September. The reason for the misperformance is an inconsistency of the autonomous camera image processing algorithm with the presence of warm pixels, i.e. pixels with increased signal rate above the mean background. This required an ad-hoc modification in the setting of the camera parameters before the entry into AFM. The performance of the navigation camera with the modified setting also showed some unexpected behaviour (CCD blooming). For a period of more than 1 hour, the camera tracking measurements of the asteroid around CA were considerably disturbed. Due to the performance problems of

the navigation camera in asteroid tracking mode, the system requirement on the S/C pointing of 0.3° was violated for some minutes shortly before CA. The maximum peak off-pointing of the nominal payload line-of-sight was 0.4° and occurred along the x-axis of the S/C (equivalent to the tracking angle in the flyby plane). The pointing along the S/C y-axis was always sufficiently accurate.

5. REFERENCES

- [1] Morley T. and Budnik F., *Rosetta Navigation for the Fly-by of Asteroid 2867 Steins*, ISSFD Toulouse, 2009.
- [2] Kueppers et al., *Determination of the light curve of the Rosetta target asteroid (2867) Steins by the OSIRIS camera onboard Rosetta*, *Astronomy & Astrophysics*, 462, L13-L16, 2007
- [3] Weissman et al., *Photometric observations of Rosetta target asteroid 2867 Steins*, *Astronomy & Astrophysics*, 466, 737-742, 2007
- [4] Fornasier et al., *First albedo determination of 2867 Steins, target of the Rosetta mission*, *Astronomy & Astrophysics*, 449, L9-L12, 2006
- [5] Bowell et al., *Application of Photometric Models to Asteroids*, Asteroids II, University of Arizona Press, 1989
- [6] Hviid S., *OSIRIS Experiment Data Record and Software Interface Specification*, RO-RIS-MPAE-ID-018, 2006
- [7] Jorda et al., *Geometric Model for the OSIRIS/NAC Camera*, Internal Report, 2005